J Neurophysiol 95: 1917–1925, 2006.
First published September 7, 2005; doi:10.1152/jn.00637.2005.

Fructose Supports Energy Metabolism of Some, But Not All, Axons in Adult Mouse Optic Nerve

Lynne Allen,[1] Susan Anderson,[2] Regina Wender,[3] Paul Meakin,[1] Bruce R. Ransom,[4] David E. Ray,[1] and Angus M. Brown[1,4]

[1]*MRC Applied Neuroscience Group, and* [2]*Imaging Unit, School of Biomedical Sciences, Queens Medical Centre, University of Nottingham, Nottingham, United Kingdom;* [3]*Departments of Anesthesiology and* [4]*Neurology, University of Washington School of Medicine, Seattle, Washington*

Submitted 20 June 2005; accepted in final form 31 August 2005

Allen, Lynne, Susan Anderson, Regina Wender, Paul Meakin, Bruce R. Ransom, David E. Ray, and Angus M. Brown. Fructose supports energy metabolism of some, but not all, axons in adult mouse optic nerve. *J Neurophysiol* 95: 1917–1925, 2006. First published September 7, 2005; doi:10.1152/jn.00637.2005. We used transmission electron microscopy (TEM) and electrophysiological techniques to characterize the morphology and stimulus-evoked compound action potential (CAP), respectively, of the adult mouse optic nerve (MON). Electrophysiological recordings demonstrated an identical CAP profile for each MON. An initial peak, smallest in area and presumably composed of the fastest-conducting axons displayed the lowest threshold for activation as expected for large axons. The second peak, the largest, was presumably composed of axons of intermediate diameter and conduction velocity, and the third peak was composed of the slowest and presumably smallest axons. In 10 mM fructose, the first CAP peak area was reduced by 78%, but the second and third peaks were unaffected. Histological analysis revealed a cross-sectional area of 33,346 μm^2, containing 24,068 axons per MON. All axons were myelinated and axon diameter ranged from 0.09 to 2.58 μm, although 80 $\pm$ 6% of the axons were $<$0.75 μm in diameter and only 0.6 $\pm$ 0.3% of the axons were $>$2 μm in diameter. After bathing in fructose for 2 h 94 $\pm$ 2% of normal appearing axons were $<$0.75 μm in diameter and none were $>$1.5 μm—all of the larger axons being grossly abnormal in structure. We conclude that fructose is unable to support function of the larger axons contributing to the first CAP peak, thus enabling us to identify a distinct population of axons that contributes to that peak.

INTRODUCTION

The rodent optic nerve, a purely myelinated central white matter tract, has served as a useful model for studying a variety of physiological and pathological processes. Its experimental advantages include that it can be easily removed intact and studied in vitro for long periods and that it has a uniform cellular structure that underlies and can be correlated with its function. The rodent optic nerve has been used to study CNS regeneration (Cho et al. 2005; Sugioka et al. 1995), the role of myelin in a model of multiple sclerosis (Waxman et al. 2004), and the effects of energy deprivation (Brown et al. 2001a; Garthwaite et al. 1999; Stys et al. 1990b). Recordings of stimulus-evoked compound action potentials (CAPs) in rodent optic nerve using suction electrodes have been used for many years to study the effects of anoxia (Stys et al. 1990b, 1992), aglycemia (Brown et al. 2001a), or ischemia (Garthwaite et al. 1999) in white matter, as CAP area (a measure of nerve conduction) is stable over time and can be accurately monitored to provide a reproducible index of injury. Comparing the ratio of CAP area before and after the insult indicates the degree of damage incurred by the nerve and also gives a benchmark against which neuroprotective strategies can be evaluated (Brown and Ransom 2002; Brown et al. 2001a,c; Fern et al. 1993, 1995; Stys et al. 1990b, 1992). More recently the latency to CAP failure after the onset of aglycemia has been used as an indicator of energy substrate levels present in rodent optic nerve. Indeed the linear relationship between the latency to CAP failure and the glycogen content of the tissue (Brown et al. 2003; Wender et al. 2000) has been useful in studying the role of glycogen in supporting nerve function.

Until recently the rat optic nerve (RON) was the preparation of choice, and its electrophysiological (Stys et al. 1991) and morphological characteristics (Fukuda et al. 1982; Hildebrand and Waxman 1984; Reese 1987) have been studied in detail. However, the mouse model is now being used in several laboratories (Brown et al. 2003; Chen et al. 2004; Weber et al. 1999) as it offers the following key advantages over the rat: it will be compatible with future transgenic models (Chen et al. 2002, 2004), which will be predominantly mouse models, and the smaller mouse optic nerve offers reduced diffusion distances from the bath perfusate to the tissue, a key consideration in studies of energy metabolism in isolated tissue, where delivery of blood borne energy substrates to the tissue is circumvented (Baltan Tekkök et al. 2003).

Brain cells use glucose as their primary substrate for ATP production. Although it is known that other hexoses can support energy metabolism in neurons (Yamane et al. 2000), there has been no evidence that neuron populations might differ in their ability to use different carbohydrate substrates. That is the point of this paper. A specific population of optic nerve axons cannot use the monosaccharide fructose to maintain excitability. This curious finding allowed us to determine for the first time exactly which population of axons contributed to the first peak of the characteristic three peaked CAP (Stys et al. 1991). While it is self evident that the three peaks must represent three populations of axons differing in conduction velocity, it has not been possible to determine with certainty which axons were the fastest conducting (i.e., those with the

Address for reprint requests and other correspondence: A. M Brown, MRC Applied Neuroscience Group, School of Biomedical Sciences, Queens Medical Centre, University of Nottingham, Nottingham, NG7 2UH, UK (E-mail: ambrown@nottingham.ac.uk).

The costs of publication of this article were defrayed in part by the payment of page charges. The article must therefore be hereby marked "*advertisement*" in accordance with 18 U.S.C. Section 1734 solely to indicate this fact.

largest diameter, those with the thickest myelin sheathes, those with the greatest internodal distance). This mystery is solved when fructose is the sole energy substrate for the optic nerve axon; only the first peak is lost, the second and third peaks are unaffected. This enabled us to identify for the first time a distinct population of axons based on diameter that contribute to an individual CAP peak.

METHODS

All procedures were carried out in accordance with the Animals (Scientific Procedures) Act 1986 under appropriate authority of project and personal licenses.

Electrophysiology

Adult male CD-1 mice (35–45 g: ≥56 day) were obtained from Charles Rivers, UK. The mice were killed by cervical dislocation and then decapitated. Optic nerves were dissected free and cut at the optic chiasm and behind the orbit. The optic nerves were gently freed from their dural sheaths and placed in an interface perfusion chamber (Medical Systems, Greenvale, NY), maintained at 37°C, and superfused with artificial cerebrospinal fluid (ACSF) containing (in mM) 126 NaCl, 3.0 KCl, 2.0 $CaCl_2$, 2.0 $MgCl_2$, 1.2 NaH_2PO_4, 26 $NaHCO_3$, and 10 glucose. In some experiments, 10 mM fructose was substituted for 10 mM glucose. The chamber was continuously aerated by a humidified gas mixture of 95% O_2-5% CO_2. After dissection, optic nerves were allowed to equilibrate in standard ACSF for ~30 min before beginning an experiment. Suction electrodes back-filled with the appropriate ACSF were used for stimulation and recording. One electrode was attached to the rostral end of the nerve for stimulation, and the second suction electrode was attached to the proximal end of the nerve to record the CAP, thus all recordings were orthodromic. Stimulus pulse strength (30 μs duration, Grass S88 dual output square pulse stimulator in combination with an SIU5 RF stimulus isolation unit, Grass, Astro-Med, Slough, UK) was adjusted to evoke the maximum CAP possible and then increased another 25% (i.e., supramaximal stimulation). During an experiment, the supramaximal CAP was elicited every 10 s. The recording electrode was connected to an Axoprobe 1A amplifier, the conditioned differential output (10×) of which was amplified 100× (Tektronix D13 Dual Beam Conditioning Oscilloscope with 5A18N Dual Trace Amplifier), filtered at 30 kHz, and acquired at 20 kHz.

Data analysis and curve fitting

Optic nerve axon function was monitored quantitatively as the area under the CAP, which represents the best measure of the number of active axons as currents generated by individual axons within a fiber tract are considered to sum (Cummins et al. 1979; Stys et al. 1991). Data were acquired on-line (Axon Instruments, Digidata 1200A) using proprietary software (Axon Instruments, Axotape). The three individual peaks of the CAP were described by individual Gaussian functions of the form (Clampfit 8.0, Axon Instruments)

$$y = \frac{A}{w\sqrt{\frac{\pi}{2}}} e^{-2\frac{(\text{time}-c)^2}{w^2}} \quad (1)$$

where A = peak area, w = width of peak at half-maximum amplitude, and c = latency to maximum amplitude of the peak.

Transmission electron microscopy (TEM)

Mouse optic nerves (MONs) were dissected as described in the preceding text, laid out on cardboard and fixed in 2% glutaraldehyde and 2% paraformaldehyde solution in 0.2 M phosphate buffer overnight and postfixed in 1% osmium tetroxide for 30 min. They were dehydrated in a graded ethanol series and embedded in Transmit low-viscosity resin (TAAB). Semi-thin sections were cut at 0.5 μm, stained with toluidine blue, and photographed using a Leica DM400B light microscope with color digital camera and Openlab darkroom software. Ultrathin sections (70–90 nm) were prepared using a Reichert-Jung Ultracut E ultramicrotome and mounted on 100 hexagonal copper grids. They were contrasted using uranyl acetate and lead citrate and viewed using a JEOL 1010 TEM operated at 80 kV with digital image acquisition.

Estimates of axon count and diameter

A low-magnification image (×300) of the cross-section of the entire MON was recorded to measure total MON area. The hexagonal grid was used to obtain a systematic random selection of areas (Mayhew and Sharma 1984) to record at the higher magnification (10,000×). For the first MON analyzed, a maximum of seven distinct fields (18.8 × 12.5 μm) were recorded per hexagon as illustrated in Fig. 5, one in each corner and one in the center, dependent on the degree of overlap between the hexagonal grid and the MON. The samples were focused at 20,000× to minimize the effect of hysteresis. The actual count of axons was carried out in a smaller region of interest (ROI, 9.0 × 6.33 μm: total area 56 μm^2, as illustrated in Fig. 5*B*) within this area to allow reliable assessment of which axons were >50% inside the ROI. The internal diameter of each axon judged to be inside each ROI was measured using Openlab software (Improvision). Simple proportion calculations allow us to estimate the number of axons in the entire MON given the total areas of the ROIs and the number of axons they contained. This method of counting was laborious and took over 7 h for a single MON. A faster method has been developed that allows counting of fewer ROIs while still maintaining accuracy of the total estimate (Mayhew and Sharma 1984). We applied this technique to the nerve illustrated in Fig. 5 but only counted two ROIs per hexagon instead of seven. Using this method, our estimate of the number of axons was 22,236 compared with 22,337 using the more laborious method described in the preceding text, validating its use. We used this counting method to estimate the number of axons in the remaining MONs described in this study. In fructose-treated nerves, we chose as a criterion to exclude any axons from the count which had a decreased density of staining indicating decreased neurofilament density, swollen mitochondria and edematous and vacuolated axons (King 1999).

Data analysis

Data are presented as means ± SD. Significance was determined using Student's *t*-test, where $P < 0.05$ was taken to indicate statistical significance. NS. indicates significance was not reached.

RESULTS

Ability of fructose to sustain the CAP

It has been shown that the rodent optic nerve can survive for extended periods of time on nonglucose metabolites, such as lactate, pyruvate, and mannose (Brown et al. 2001b). Therefore we extended our previous study by determining the ability of fructose to sustain axon function in the adult MON by monitoring the CAP every 10 s in the presence of fructose. In the presence of 10 mM glucose, the CAP can be sustained for several hours (Fig. 1*A*) (Brown et al. 2001b). When 10 mM glucose in the ACSF was replaced by 10 mM fructose, the CAP area was sustained for ~30 min after which time it began to fall (Fig. 1*A*). Analysis of the individual CAP peaks showed that in the presence of 10 mM glucose, the CAPs displayed the

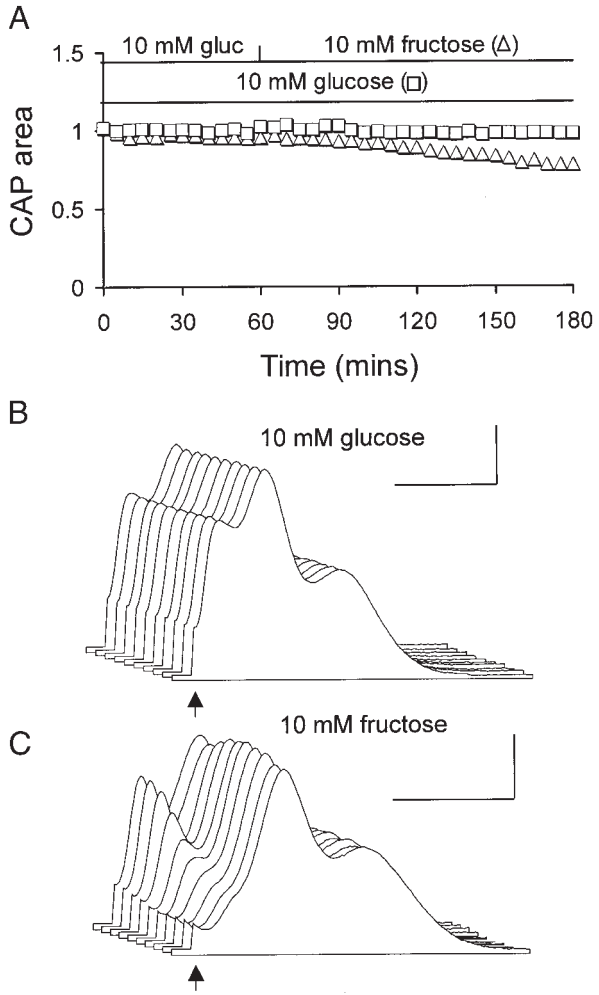

FIG. 1. The ability of fructose to support the compound action potential (CAP). *A*: in the presence of 10 mM glucose, the CAP is very stable (□), but 10 mM fructose causes a decrease in the CAP area about 30 min after introduction (△). *B*: sequential display illustrates the stability of CAPs recorded in 10 mM glucose, where the most recent CAPs are at the front of the *z* axis. *C*: in 10 mM fructose, sequential display of CAPs demonstrates the gradual loss of the 1st peak. The 1st CAP peak was recorded 30 min after the introduction of 10 mM fructose, and CAPs displayed were recorded at 1-min intervals. Scale bars are 1 mV and 1 ms for *B* and *C;* ↑, stimulus. Stimulus artifacts have been removed for clarity.

three peaks typical of the rodent preparation (Brown et al. 2003; Stys et al. 1991) and over time displayed very little variation (Fig. 1*B*). However, in the presence of fructose, it was apparent that the first of the three CAP peaks was gradually lost, although the 2nd and 3rd peaks were unaffected (Fig. 1*C*). This selective effect of fructose on an individual CAP peak, which was also seen in the RON but not investigated at the time (Brown et al. 2001b), prompted us to quantify each of the three peaks of the CAP using electrophysiological techniques.

Electrophysiological profile of the stimulus-evoked CAP

The three-peaked CAP evoked by supramaximal stimulus of the MON is typical of the rodent preparation and is illustrated in Fig. 2. In all MONs tested, the profile was always qualitatively identical with the 2nd peak being the largest, demonstrating that the CAP is a reliable and stable index of axon conduction. Each individual peak was well fit by a Gaussian function (Fig. 2, *inset*), strongly suggesting that each peak reflects a distinct population of axons. In recordings from 29 MONs, the total CAP area varied from 2.62 to 8.42 mV ms. Plotting the area of each of the three peaks illustrated the contribution of each peak to the total CAP area. The area of the 1st CAP peak was 0.90 ± 0.31 mV ms, the 2nd CAP peak 2.71 ± 0.87 mV ms, and the 3rd CAP peak 1.66 ± 0.65 mV ms. The latency to the maximum amplitude of the 1st CAP peak (c in *Eq. 1*, METHODS) was 1.39 ± 0.08 ms, to the 2nd CAP peak 1.74 ± 0.15 ms, and to the 3rd CAP peak 2.37 ± 0.17 ms.

Relationship between stimulus intensity and CAP profile

Figure 3, *A* and *B,* illustrates the relationship between the stimulus intensity and the CAP. In Fig. 3*A,* the *z* axis denotes the stimulus voltage, which increased in 0.15 V increments from 0 to 3 V. It is evident that increasing the stimulus voltage augments the CAP, i.e., as the stimulus voltage is increased the CAP becomes larger. The nature of this increase is as follows. A peak emerges at ~0.45 V stimulus voltage, ~1.40 ms from the stimulus artifact, and this peak is named the 1st CAP peak. As the stimulus voltage is further increased a second peak, distinct from the first CAP peak, is evoked at 1.2 V stimulus voltage and peaks at ~1.75 ms after the stimulus artifact, and this is named the 2nd CAP peak. At stimulus voltages of 2.5 V, a third distinct peak is evoked ~2.4 ms after the stimulus, and this is named the 3rd CAP peak (Fig. 3, *A* and *B*). Measurement of the areas of each of the individual CAP peaks plotted against stimulus voltage demonstrated two key points (Fig. 3*C*, $n = 4$). First, the 1st CAP peak displays the lowest threshold for recruitment, the 2nd CAP peak has an intermediate recruitment threshold, and the 3rd CAP peak is recruited last. Second, the 1st CAP peak contributes 17.1% to the total CAP area at supramaximal stimuli, the 2nd CAP peak 51.4%, and the 3rd CAP peak 31.5%. By normalizing the area of each of the peaks, it is clear that the CAP area versus stimulus voltage curves do not overlap for each of the peaks, suggesting that the axons that contribute to each CAP possess distinct characteristics (Fig. 3*D*). This was further emphasized by the data shown in Fig. 3*E*, where the latency to maximum amplitude of each peak is plotted against the area of each peak (parameters *c* and *A,* respectively, in *Eq. 1*, METHODS). It is apparent that each peak represents a discrete population of axons with no overlap between the latency to maximum amplitude of each of the peaks. Figure 3*F* illustrates the percentage contribution of

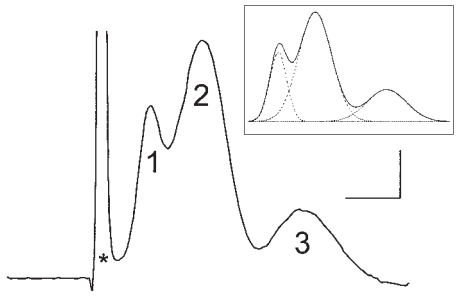

FIG. 2. Characteristics of a CAP evoked by supramaximal stimulus. The CAP is composed of 3 peaks, an initial 1st peak (1), followed by a larger 2nd peak (2), and a smaller 3rd peak (3); the initial large peak is the stimulus artifact, (*). Scale bars are 1 mV and 1 ms. *Inset*: bold image represents a recorded CAP and the dotted lines represent the best fit Gaussian function of each of the 3 peaks.

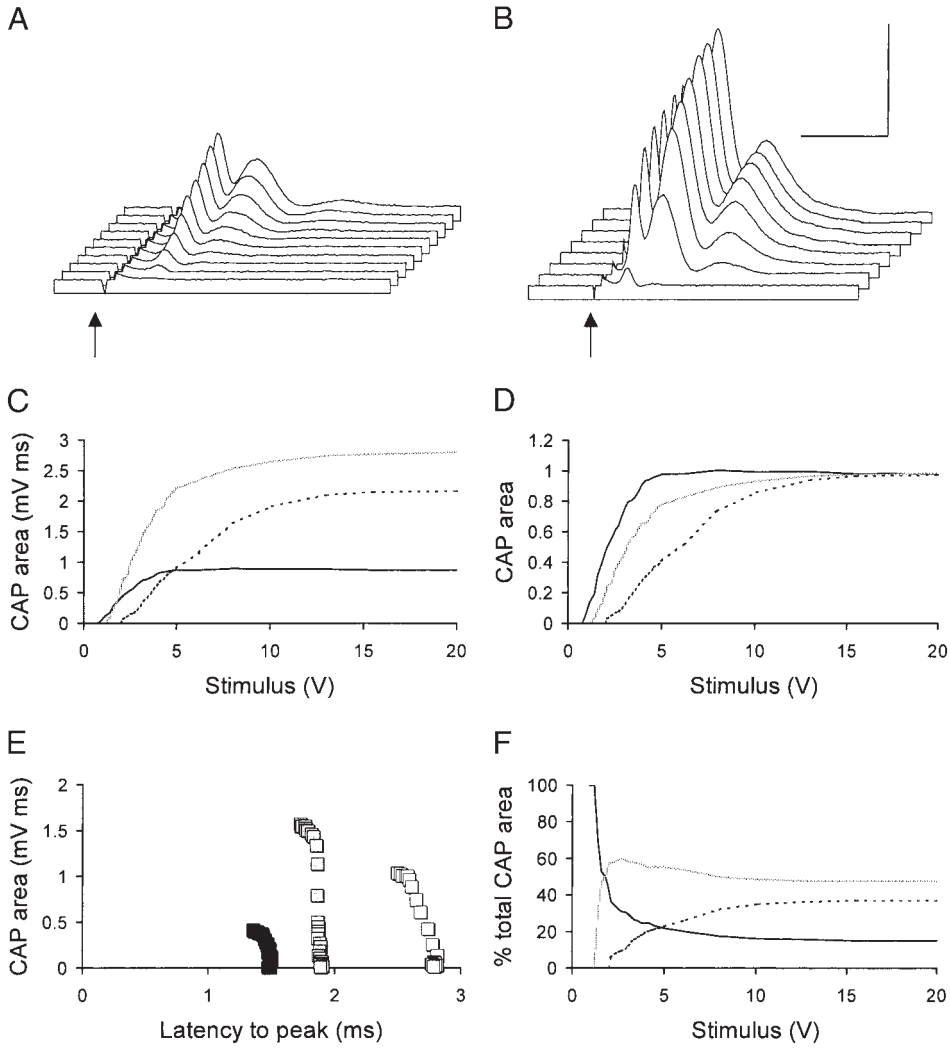

FIG. 3. Electrophysiological characteristics of the stimulus evoked CAP. *A*: successive voltage stimuli in 0.45 V steps from 0 V (*z* axis) elicited an increasing CAP. A peak with the shortest latency, i.e., fastest conduction velocity was evoked 1st (1st CAP peak), followed by a 2nd (2nd CAP peak), then a 3rd peak (3rd CAP peak). *B*: similar to *A* except that the stimuli were evoked in 6 V steps and demonstrates the late development of 3rd CAP peak. The scale bars are 2 mV and 1 ms and apply to both *A* and *B;* ↑, stimulus. Stimulus artifacts have been removed for clarity. *C*: plot of the stimulus voltage vs. the CAP peak area. The 1st CAP peak (black) is evoked first but contributes the smallest area of the 3 peaks. The 2nd CAP peak is recruited next but contributes the most toward the total CAP area (▨). The 3rd CAP peak is recruited last and contributes the 2nd largest area (· · ·). *D*: normalizing the data from *C* highlights both the threshold voltage at which each CAP peak is evoked, and the growth of each CAP peak area in response to increasing stimulus voltage. *E*: relationship between the latency to the maximum value of each CAP peak vs. CAP peak area indicates that each CAP peak belongs to a distinct population of axons. *F*: plotting the contribution of each CAP peak to the total CAP area vs. stimulus voltage illustrates the importance of imposing a supramaximal stimulus to recruit all available axons. The data markers described in *C* also apply to *D* and *F*.

each peak to the total CAP area versus stimulus voltage. Given that the 1st CAP peak has the lowest threshold and is thus recruited first, at the lower stimulus voltages the 1st CAP peak contributes significantly to the total CAP area, but as the stimulus voltage is increased and the remaining axons are recruited, the 2nd and 3rd CAP peaks dominate, until after 15 V, a stable value for each has been reached. This emphasizes the key point that a supramaximal stimulus must be employed for an accurate representation of all available axons (Stys et al. 1991).

Effects on of fructose on individual CAP peaks

Detailed analysis revealed that in the presence of 10 mM glucose over a period of several hours, the CAP remained stable, with each of the individual CAP peaks unaltered (Fig. 4*A*). However, in the presence of 10 mM fructose, the 1st CAP peak decreased, but the 2nd and 3rd CAP peaks were unchanged (Fig. 4*B*). After 2 h in the presence of 10 mM fructose, the 1st CAP peak area had decreased from 0.72 ± 0.27 to 0.16 ± 0.09 mV ms ($P < 0.005$), whereas the 2nd (1.59 ± 0.43 vs. 1.38 ± 0.43 mV ms, NS) and 3rd CAP peaks (0.99 ± 0.38 vs.1.12 ± 0.33 mV ms, NS) were not affected (Fig. 4*C*, $n = 5$), suggesting that the axons contributing to the 1st CAP peak are incapable of metabolizing fructose, whereas those contributing to the 2nd and 3rd CAP peaks are capable of efficiently metabolizing fructose.

Electron microscopic observations of MONs

MONs showed good preservation under both light and electron microscopic observation in control conditions. Figure 5*A* illustrates a light micrograph of an entire MON with an outline of the hexagonal grid superimposed. In this example, the MON was contained within eight hexagons, each of which contained between two and seven ROIs. The number and diameter of axons contained within each ROI was measured. The coefficient of variation (SD/mean * 100%) for each hexagonal ROI was calculated, and the similarity of these values (38.4–51.0) suggested that there was not a great variation in axon diameter within the nerve, i.e., the axon diameters were evenly distributed throughout the nerve (Mayhew and Sharma 1984). Calculations using all of the axons diameters in all 43 fields yielded a mean diameter of 0.626 μm with a coefficient of variation of 44%.

The total cross sectional area of the MON illustrated in Fig. 5*A* was 31,603 μm^2. Simple proportion calculations allow us to estimate the number of axons in the entire MON given the total

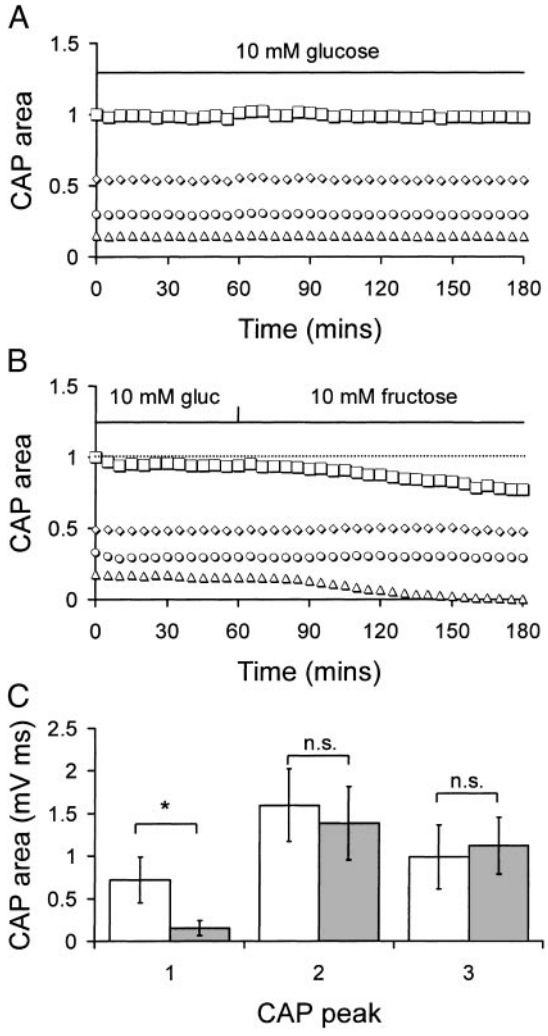

FIG. 4. The effects of fructose on individual CAP peaks. *A*: bathing MONs in 10 mM glucose resulted in stable CAPs with each of the peaks unaltered over a period of 3 h. □, the total CAP area; ◇, the 2nd CAP peak; ○, the 3rd CAP peak; and △, 1st CAP peak. This scheme also applies to *B*. *B*: MONs bathed in 10 mM fructose for 2 h displayed a loss of total CAP area, which was due to a delayed loss in the 1st CAP peak. *C*: histogram illustrating the loss of the 1st CAP peak after a 2-h incubation in 10 mM fructose, whereas the 2nd and 3rd CAP peaks were not significantly affected. □, MONs bathed in 10 mM glucose for 2 h; ▨, MONs bathed in 10 mM fructose for 2 h. $*P < 0.005$; NS, not significant.

area of the ROIs and the number of axons they contained: i.e., if 2408 μm^2 (43 ROIs of 56 μm^2 each) of measured MON area contains 1,702 axons, then the entire MON (31,603 μm^2) contains 22,337 axons. Employing the method of counting requiring only two ROIs per hexagon gave estimates of axon number at 22,236. In the two other control MONs analyzed, the total areas were 36,089 and 32,345 μm^2, respectively, which contained 25,891 and 23,835 axons, respectively. Calculations using data from each of the three control MONs yielded a between MON coefficient of variation of 7.4% for the axon diameter and 7.6% for the number of axons.

In addition to the number of axons contained in the MON, it is of particular interest to assess the distribution of axons diameters as axon diameter is one of the chief determinants of axon conduction velocity. We plotted histograms of axon diameter from each of the three MONs demonstrating the similar distribution of axon diameter within each nerve (Fig. 6). The measurements of axon diameter from each MON were divided into 0.25 μm bins and showed that the most common axon diameter was between 0.25 and 0.75 μm (Fig. 6), with a paucity of axon diameters <0.25 μm as previously described (Waxman and Bennett 1972).

Effect of incubation in 10 mM fructose for 2 h on axon morphology

After MONs were incubated in 10 mM fructose for 2 h, there were obvious differences when compared with control axons, which had been incubated in 10 mM glucose for the same period of time. The larger-diameter axons were swollen and edematous and displayed vacuolization (Fig. 7, *C* and *D*). However, the smaller axons appeared to be relatively unaffected. Plotting frequency histograms of viable axons from control and fructose-treated MONs illustrated that there was a loss of the contribution of axons over 0.75 μm in MONs treated with fructose. Our criteria to determine axon viability were as follows. In Fig. 7, *A* and *B,* all axons appear of uniform density of staining and exhibit mitochondria of uniform appearance. However, it is clear from Fig. 7, *C* and *D,* that incubation in fructose has had a significant effect of some axons. In particular, the density of staining in larger axons is lighter than in smaller axons indicating a decreased density of microtubules. Additionally mitochondria in these lightly stained larger axons appear swollen, and some axons appear edematous and vacuolated. Axons which displayed any of these characteristics, were omitted from the count as they were judged to display evidence of pathology (King 1999). In control conditions, 20.2 ± 6.3% of axons were over 0.75 μm in diameter (Fig. 8*A*), whereas in the fructose-treated animals, only 5.6 ± 1.6% were over 0.75 μm in diameter (Fig. 8*B*). This loss of larger axons is consistent with the larger-diameter axons contributing to the 1st peak of the CAP and hence their loss in the presence of fructose.

DISCUSSION

This present study extends our knowledge of the rodent optic nerve preparation by quantifying key characteristics of the adult MON and demonstrating a unique metabolism of a subpopulation of axons, which were unable to metabolize fructose. Electrophysiological techniques were used to quantify each of the three peaks that contribute to the CAP by determining both the area, and hence the contribution of each peak to the total CAP area, and latency to the maximum amplitude of each peak. In each of the 29 MONs recorded, CAPs were qualitatively identical, i.e., they were composed of three peaks of which the second was largest. TEM techniques were used to estimate the number of axons in each MON, and the results were consistent in each of the three control nerves tested. Histograms of axon diameter revealed that ~80% of axons had diameters of <0.75 μm. Bathing MONs in fructose resulted in delayed loss of the first peak of the CAP and electron micrographs of treated MONs revealed a loss of axons over 0.75 μm in diameter, demonstrating that axons of a known diameter contribute to an individual peak of the CAP.

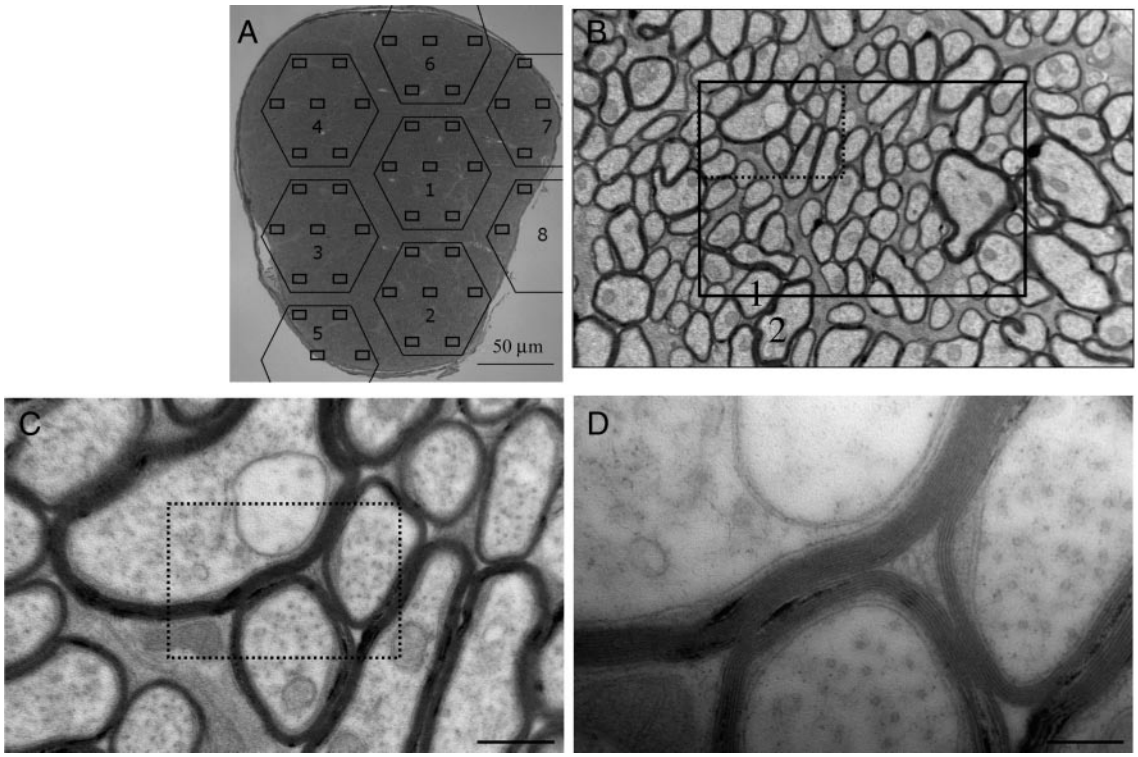

FIG. 5. Electron micrographs (EMs) of the MON. *A*: whole cross-section of a MON is displayed on the hexagonal template. The small rectangles within each hexagon indicate the fields used in the count. *B*: higher-power pictograph of one of the fields indicated in *A*. The smaller rectangle indicates the region of interest (ROI) in which the axon diameters were counted. Only axons which had half of their areas or more within the rectangle were included in the count, thus the axon marked 1 was included, but the axon marked *2* was excluded from the count. Scale bar 2 μm. *C*: EM pictograph of the dotted area in *B* demonstrating myelination and evenly spaced cytoplasmic mitochondria and microtubules. Scale bar 0.5 μm. *D*: EM pictograph of the dotted area in *C* illustrating individual successive wraps of myelin can be clearly seen on each of the 4 axons illustrated. Scale bar: 0.2 μm.

Fructose metabolism

The vast majority of previous studies, which have used the CAP as a monitor of axon conduction, used the entire CAP area as in the experimental maneuvers carried out, there was no significant difference in the response of each of the peaks (Brown et al. 2003; Fern et al. 1996; Garthwaite et al. 1999; Stys et al. 1990a; Sugioka et al. 1995). It has been known for many years that fructose can support function in isolated brain preparations, where it was assumed that hexokinase phosphorylated the fructose (McIlwain and Bachelard 1985). Both the V_{max} (25 vs.17 μmol $\cdot$ min^{-1} $\cdot$ g^{-1}) and K_m (1 mM vs.10 μM) are greater for fructose than for glucose, hence hexokinase has a lower affinity for fructose but larger capacity (Newsholme and Leech 1983). However, given the substrate concentrations used in our experiments (10 mM), both should be phosphorylated at maximal activity. The even distribution of all axon diameters throughout the MON suggests that the inability of fructose to support the first CAP peak is not due to diffusion differences as fructose will have equal access to all axons [the 30-min lag period between the introduction of fructose and 1st CAP peak failure is due to reserves of glycogen sustaining function. Once the glycogen is depleted function fails (Meakin, Rathbone, Allen, Ransom, Ray, and Brown, unpublished data)]. It has been argued that the partial ability of fructose to support neuronal function in hippocampal slices is largely a glycolytic effect and that although fructose can support ATP levels, it cannot fully support neural activity with glucose an absolute requirement for neural activity (Yamane et al. 2000). This is clearly not the case in the MON where the 2nd and 3rd CAP peaks are fully supported by fructose for extended periods of time.

Possible explanations for the differential effect of fructose on the CAP peaks include *1*) 1st CAP peak axons do not, whereas the 2nd and 3rd CAP peak axons do, express the GLUT5 transporter which transports fructose across cell membranes. *2*) 1st peak CAP axons do not express the enzyme fructokinase, which phosphorylates fructose in liver and kidney, whereas the 2nd and 3rd CAP peak axons do express the enzyme. This may be feasible if the V_{max} for fructose was a lot higher for fructokinase than hexokinase, thus the ability of the 2nd and 3rd CAP peak axons to thrive in the presence of fructose is due to the presence of a high capacity fructokinase. 1st CAP peak axons only possess hexokinase, which due to its low V_{max}, is incapable of generating sufficient ATP to fully support CAP conduction. All axons obviously contain hexokinase as they can efficiently metabolize glucose—it is extremely unlikely that the axons differentially express isoforms of hexokinase that differ in their kinetics. Although not addressed in this paper these questions are currently under investigation in our laboratory.

Electrophysiological characterization of the stimulus-evoked CAP

The electrophysiological characteristics of the stimulus evoked CAP have been extensively characterized in rat (Stys et al. 1991), and this initial work demonstrated the critical importance of a tight seal around both the stimulus electrode and the recording electrode; a loose seal at the recording electrode

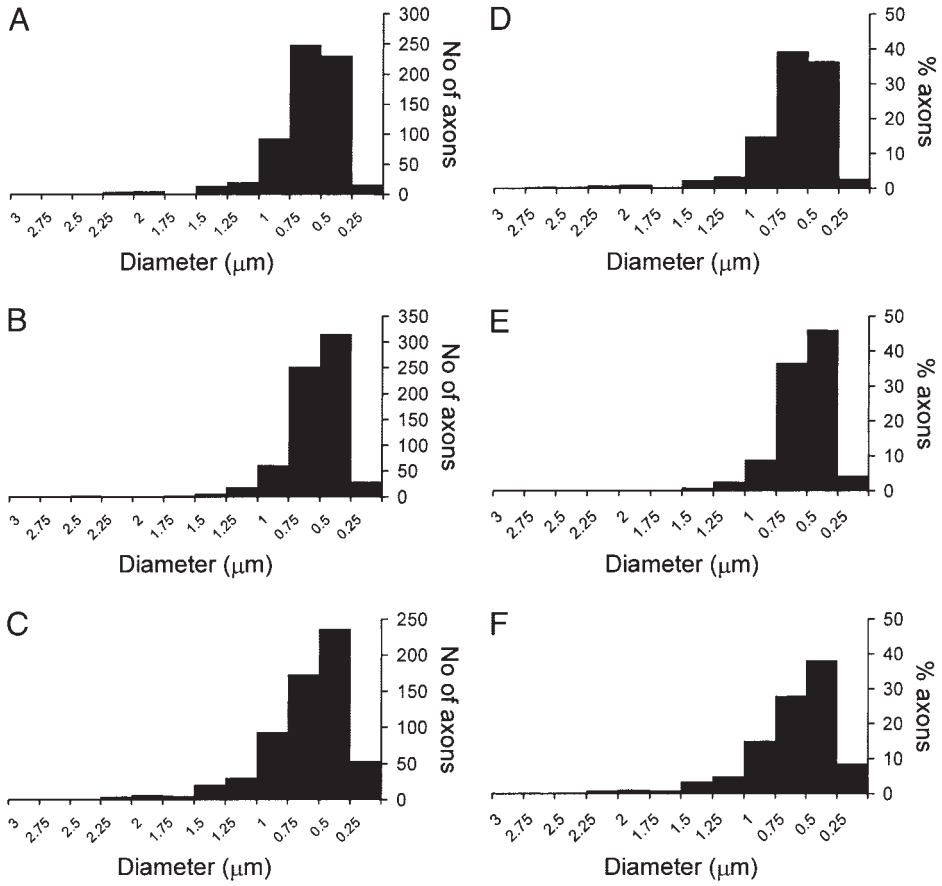

FIG. 6. Histograms of axon diameter in 3 control MONs. *A*: in MON 1, the majority of axons were in the 0.25- to 0.75-μm-diam range, with only a small percentage of axons >1 mm. Similar results were seen in the 2 other MONs studied (*B* and *C*). *D*—*F*: plotting the data from *A* to *C* as percentage contribution of each of the 0.25-μm bins to the total axon population, reveals that the majority of axons are between 0.25 and 0.75 μm in diameter.

leads to electrical shunting and attenuation of the signal (Stys and Kocsis 1995), whereas a loose seal at the stimulus electrode leads to a continually increasing CAP area with stimulus voltage rather than a plateau as reached with higher-resistance seals (Stys et al. 1991). Although this initial pioneering work was carried out in rat it applies equally to mouse. The three peaks of the CAP that we recorded in response to the supramaximal stimulus are typical of the rodent preparation and are seen in both rat (Garthwaite et al. 1999; Stys et al. 1991; Sugioka et al. 1995) and other strains of mouse (Brown et al. 2003; Chen et al. 2004; Weber et al. 1999). It is hypothesized that each distinct peak of the CAP is a result of distinct types of retinal ganglion cell, the cell bodies of the optic nerve axons (Stone 1983). Our TEM studies have indicated that, as in the rat (Waxman et al. 1990), all of the axons in the adult animal are myelinated. The response of the MON to increasing stimulus demonstrated that each peak was composed of axons that had different thresholds for activation. As all axons are myelinated this difference in threshold is likely due to axon diameter although it could also be due to differences in internodal distance or Na^+ channel density at the node. If we imagine a MON axon of a small diameter, e.g., 0.25 μm, then doubling the diameter of the axon to 0.50 μm will result in the internal resistance (r_i) decreasing to a greater degree than the membrane resistance (r_m), as r_i varies with the square of the diameter, whereas r_m varies linearly with the diameter ($r_i = R_i/\pi a^2$: $r_m = R_m/2\pi a$). Thus increasing axon diameter results in less stimulating voltage being required to evoke a response than in a smaller axon, hence the lower threshold required to evoke a response in large axons (Nicholls et al. 1992).

Our data show that each of the three peaks can be modeled by a Gaussian function. Traditionally Gaussian functions have been used to describe the normal distribution of a particular parameter in a population. Because the CAP is composed of three Gaussian functions, this suggests that the axons that contribute to each peak represent a distinct population. The fact that some of the peaks overlap indicates that although some of the axon diameters are shared between two different populations, they have distinct characteristics as evidenced by the fact that fructose results in a loss of the 1st CAP peak but the axons overlapping between peaks 1 and 2 are not killed.

MON axon diameter and count

To estimate the number of axons in the MON, we used a method developed to count axons in peripheral nerve bundles (Mayhew and Sharma 1984). This method was demonstrated to accurately estimate the number of axons in nerve bundles by counting relatively few of the axons within the preparation but using a scaling method to estimate the total count. In the one MON in which we used the method where we counted either seven ROIs or two ROIs per hexagon, there was an excellent agreement in the number of axons estimated (22,236 vs.22,337), validating the use of the reduced ROI estimate procedure. Previous studies have shown that there are ~1.1 million axons in the human optic nerve, 100,000 in the rat, and 86,000 in the cat (Mayhew and Sharma 1984). Our estimates of

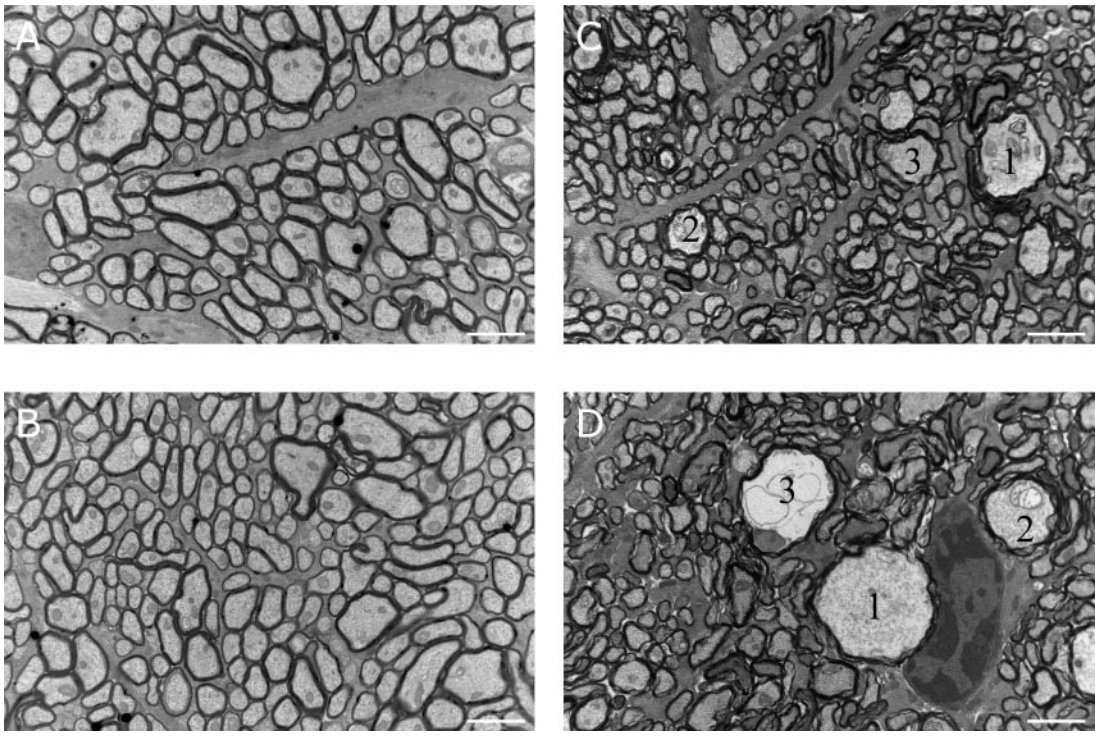

FIG. 7. EMs of the control and fructose-treated MONs. *A* and *B*: control MONs contained axons of which 100% were myelinated. Mitochondria and filaments could be seen within the axon cytoplasm. *C* and *D*: in fructose-treated MONs, the larger axons appeared vacuolated and edematous. However, the smaller axons appeared to be unaffected. Scale bar 2 μm. In *C* the axons marked 1 and 2 displayed a decreased density of staining and swollen mitochondria, whereas the axon marked 3, although of large diameter, was considered normal. In *D,* the axon marked 1 displayed a decreased density of staining, as did the axon marked 2, which also displayed swollen mitochondria. The axon marked 3 was edematous and displayed vacuolisation

the number of axons in the MON (~24,000), is within the range expected based on data from the rat, given that the MON diameter we measured was ~240 μm and the RON diameter is about double this (Baltan Tekkök et al. 2003). Thus the MON area is about a quarter that of the RON and contains about a quarter the number of axons. This of course assumes that the axons in the MON are in the same range of diameters as in the rat, which appears to be the case when comparing Fig. 6 in this paper with Fig. 2 in Reese (1987). Based on the mean and coefficient of variation calculations axons of all diameter appear to be fairly uniformly distributed throughout the nerve, and this may in turn reflect the uniform distribution of ganglion cell types on the ganglion cell layer of the retina.

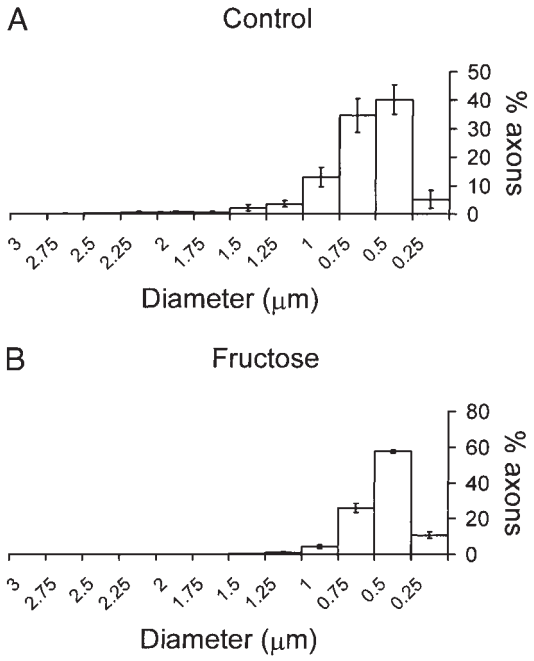

FIG. 8. Histograms of axon diameter in control and fructose treated MONs. *A*: in control MONs, the majority of the axons were between 0.25 and 0.75 μm in diameter, although a significant percentage were >0.75 μm. *B*: in fructose-treated MONs. the number of axons >0.75 μm in diameter was significantly reduced.

The shape of the CAP suggests that there are three distinct populations of axon. However, the axon diameter histograms in Fig. 6 do not show three separate populations of axon based on axon diameter, but rather the distribution is unimodal and skewed in the direction of larger axons. Thus there is obviously an overlap in the diameter of axons contribution to each peak. An additional complication is that each axons' contribution to the total CAP area is not linear but is dependent on diameter, as larger-diameter axons, due to their large membrane area and lower internal resistance, generate more current and larger extracellular voltages than small axons (Nicholls et al. 1992).

What we have shown is that in the MON, a central white matter tract, a subpopulation of axons are incapable of surviving on an energy substrate that supports the remaining axons in the preparation and, further, that these particular axons can be identified based on their conduction velocities. We can therefore definitively state that the axons contributing to the first peak of the CAP are of large diameter. Thus in the MON we conclude that neighboring axons differ in their ability to efficiently metabolize potential energy substrates via mechanisms as yet unknown.

ACKNOWLEDGMENTS

The authors thank Professor Terry Mayhew for advice on the efficient method for counting axons and J. Banks and Dr. Alistair Mathie for the generous donation of equipment. We thank K. A. Draper Morgan for additional support.

GRANTS

This work was funded by the Medical Research Council.

REFERENCES

Baltan Tekkök S, Brown AM, and Ransom BR. Axon function persists during anoxia in mammalian white matter. *J Cerebl Blood Flow Metab* 23: 1340–1348, 2003.

Brown AM, Baltan Tekkök S, and Ransom BR. Glycogen regulation and functional role in mouse white matter. *J Physiol* 549. 2: 501–512, 2003.

Brown AM and Ransom BR. Neuroprotective effects of increased extracellular Ca^{2+} during aglycemia in white matter. *J Neurophysiol* 88: 1302–1307, 2002.

Brown AM, Wender R, and Ransom BR. Ionic mechanisms of aglycemic axon injury in mammalian central white matter. *J Cereb Blood Flow Met* 21: 385–395, 2001a.

Brown AM, Wender R, and Ransom BR. Metabolic substrates other than glucose support axon function in central white matter. *J Neurosci Res* 66: 839–843, 2001b.

Brown AM, Westenbroek RE, Catterall WA, and Ransom BR. Axonal L-type Ca^{2+} channels and anoxic injury in rat CNS white matter. *J Neurophysiol* 85: 900–911, 2001c.

Chen C, Bharucha V, Chen Y, Westenbroek RE, Brown A, Malhotra JD, Jones D, Avery C, Gillespie PJ, 3rd, Kazen-Gillespie KA, Kazarinova-Noyes K, Shrager P, Saunders TL, Macdonald RL, Ransom BR, Scheuer T, Catterall WA, and Isom LL. Reduced sodium channel density, altered voltage dependence of inactivation, and increased susceptibility to seizures in mice lacking sodium channel beta 2-subunits. *Proc Natl Acad Sci USA* 99: 17072–17077, 2002.

Chen C, Westenbroek RE, Xu X, Edwards CA, Sorenson DR, Chen Y, McEwen DP, O'Malley HA, Bharucha V, Meadows LS, Knudsen GA, Vilaythong A, Noebels JL, Saunders TL, Scheuer T, Shrager P, Catterall WA, and Isom LL. Mice lacking sodium channel beta1 subunits display defects in neuronal excitability, sodium channel expression, and nodal architecture. *J Neurosci* 24: 4030–4042, 2004.

Cho KS, Yang L, Lu B, Feng Ma H, Huang X, Pekny M, and Chen DF. Re-establishing the regenerative potential of central nervous system axons in postnatal mice. *J Cell Sci* 118: 863–872, 2005.

Cummins KL, Perkel DH, and Dorfman LJ. Nerve fiber conduction-velocity distributions. I. Estimation based on the single-fiber and compound action potentials. *Electroencephalogr Clin Neurophysiol* 46: 634–646, 1979.

Fern R, Black JA, Ransom BR, and Waxman SG. Cd^{2+}-induced injury in CNS white matter. *J Neurophysiol* 76: 3264–3273, 1996.

Fern R, Ransom BR, Stys PK, and Waxman SG. Pharmacological protection of CNS white matter during anoxia: actions of phenytoin, carbamazepine and diazepam. *J Pharmacol Exp Ther* 266: 1549–1555, 1993.

Fern R, Waxman SG, and Ransom BR. Endogenous GABA attenuates CNS white matter dysfunction following anoxia. *J Neurosci* 15: 699–708, 1995.

Fukuda Y, Sugimoto T, and Shirokawa T. Strain differences in quantitative analysis of the rat optic nerve. *Exp Neurol* 75: 525–532, 1982.

Garthwaite G, Brown G, Batchelor AM, Goodwin DA, and Garthwaite J. Mechanisms of ischaemic damage to central white matter axons: a quantitative histological analysis using rat optic nerve. *Neuroscience* 94: 1219–1230, 1999.

Hildebrand C and Waxman SG. Postnatal differentiation of rat optic nerve fibers: electron microscopic observations on the development of nodes of Ranvier and axoglial relations. *J Comp Neurol* 224: 25–37, 1984.

King R. *Atlas of Peripheral Nerve Pathology.* London: Arnold, 1999.

Mayhew TM and Sharma AK. Sampling schemes for estimating nerve fiber size. I. Methods for nerve trunks of mixed fascicularity. *J Anat* 139: 45–58, 1984.

McIlwain H and Bachelard HS. *Biochemistry and the Central Nervous System.* London: Churchill Livingstone, 1985.

Newsholme EA and Leech AR. *Biochemistry for the Medical Sciences.* New York: Wiley, 1983.

Nicholls JG, Martin AR and Wallace BG. *From Neuron to Brain.* Sunderland, MA: Sinauer, 1992.

Reese BE. The distribution of axons according to diameter in the optic nerve and optic tract of the rat. *Neuroscience* 22: 1015–1024, 1987.

Stone J. *Parallel Processing in the Visual System.* New York: Plenum, 1983.

Stys PK and Kocsis JD. Electrophysiological approaches to the study of axons. In: *The Axon*, edited by Waxman SG, Kocisi JD, and Stys PK. Oxford, UK: Oxford Univ. Press, 1995, p. 328–340.

Stys PK, Ransom BR, and Waxman SG. Effects of polyvalent cations and dihydropyridine calcium channel blockers on recovery of CNS white matter from anoxia. *Neurosci Lett* 115: 293–299, 1990a.

Stys PK, Ransom BR, and Waxman SG. Compound action potential of nerve recorded by suction electrode: a theoretical and experimental analysis. *Brain Res* 546: 18–32, 1991.

Stys PK, Ransom BR, Waxman SG, and Davis PK. Role of extracellular calcium in anoxic injury of mammalian central white matter. *Proc Natl Acad Sci USA* 87: 4212–4216, 1990b.

Stys PK, Waxman SG, and Ransom BR. Ionic mechanisms of anoxic injury in mammalian CNS white matter: role of Na^+ channels and Na^+-Ca^{2+} exchanger. *J Neurosci* 12: 430–439, 1992.

Sugioka M, Sawai H, Adachi E, and Fukuda Y. Changes of compound action potentials in retrograde axonal degeneration of rat optic nerve. *Exp Neurol* 132: 262–270, 1995.

Waxman SG and Bennett MV. Relative conduction velocities of small myelinated and non-myelinated fibres in the central nervous system. *Nat New Biol* 238: 217–219, 1972.

Waxman SG, Black JA, Duncan ID, and Ransom BR. Macromolecular structure of axon membrane and action potential conduction in myelin deficient and myelin deficient heterozygote rat optic nerves. *J Neurocytol* 19: 11–28, 1990.

Waxman SG, Craner MJ, and Black JA. Na^+ channel expression along axons in multiple sclerosis and its models. *Trends Pharmacol Sci* 25: 584–591, 2004.

Weber P, Bartsch U, Rasband MN, Czaniera R, Lang Y, Bluethmann H, Margolis RU, Levinson SR, Shrager P, Montag D, and Schachner M. Mice deficient for tenascin-R display alterations of the extracellular matrix and decreased axonal conduction velocities in the CNS. *J Neurosci* 19: 4245–4262, 1999.

Wender R, Brown AM, Fern R, Swanson RA, Farrell K, and Ransom BR. Astrocytic glycogen influences axon function and survival during glucose deprivation in central white matter. *J Neurosci* 20: 6804–6810, 2000.

Yamane K, Yokono K, and Okada Y. Anaerobic glycolysis is crucial for the maintenance of neural activity in guinea pig hippocampal slices. *J Neurosci Methods* 103: 163–171, 2000.